



## Journal of Advanced Research in Fluid Mechanics and Thermal Sciences

Journal homepage:  
[https://semarakilmu.com.my/journals/index.php/fluid\\_mechanics\\_thermal\\_sciences/index](https://semarakilmu.com.my/journals/index.php/fluid_mechanics_thermal_sciences/index)  
ISSN: 2289-7879



# Heat and Mass Transfer Characteristics of Mixed Convection MHD Flow with the Impacts of Hall Current and Diffusion Thermo in the Presence of Brownian Motion and Thermophoresis

Bingi Suneetha<sup>1</sup>, Ramachandra Reddy Vaddemani<sup>2</sup>, Damodara Reddy Annapureddy<sup>3</sup>, Giulio Lorenzini<sup>4,\*</sup>

- <sup>1</sup> Department of Humanities and Sciences, G. Pullaiah College of Engineering and Technology (Autonomous), Kurnool-518001, Andhra Pradesh, India
- <sup>2</sup> Department of Humanities and Sciences, K.S.R.M College of Engineering, Kadapa, A.P 516003, India
- <sup>3</sup> Mechanical Engineering Department, JNTUACE Pulivendula-516390, Constitute College of Jawaharlal Nehru Technological University Ananthapuramu, Andhra Pradesh, India
- <sup>4</sup> Department of Engineering and Architecture, University of Parma, Parco Area delle Scienze, 181/A, 43124 Parma, Italy

### ARTICLE INFO

### ABSTRACT

#### Article history:

Received 11 November 2023  
Received in revised form 5 February 2024  
Accepted 17 February 2024  
Available online 15 March 2024

#### Keywords:

Hybrid nanofluids; chemical reaction; stretching plate; rotation parameter; Hall current; boundary layer

This study investigates the influence of Hall current diffusion, thermo-activation energy, and other parameters on the flow characteristics of an electrically conducting Jeffrey nanofluid. The Jeffrey nanofluid flow occurs across a continually expanding surface, and additional factors like thermal radiation, heat generation/absorption, and inclined plates are included in the analysis. A vertically installed transverse magnetic field is assumed to have a modest Reynolds number. The controlling partial differential equations are transformed into nonlinear ordinary differential equations using appropriate similarity transformations. These equations are then numerically solved using the Matlab `bvp4c` module. This study aims to analyze the impact of many factors, including the Hall current factor, the thermal radiation factor, the heat source/sink factor, the Brownian motion factor, the thermophoresis parameter, and the magnetization, on the velocity, concentration, and temperature. To do this, graphical representations will be used as a means of visualizing and discussing the impacts, as mentioned earlier. To get a deeper understanding of the internal dynamics of the emerging parameters, a numerical computation is conducted to determine the local Nusselt number, Sherwood number, and skin friction coefficient along the  $x$  and  $z$  axes. Research findings have shown that the flow velocity exhibits a decreasing trend as the linear and nonlinear thermal radiation components rise. Furthermore, augmenting the values of the Brownian motion parameter will lead to a reduction in the concentration profile of the nanoparticle.

## 1. Introduction

The blood flow via narrow arteries is shown by the non-Newtonian (viscoelastic) Casson fluid, which produces stress. The observation of Newtonian behaviour in blood flow from larger arterial

\* Corresponding author.

E-mail address: [giulio.lorenzini@unipr.it](mailto:giulio.lorenzini@unipr.it)

<https://doi.org/10.37934/arfmts.115.1.5168>

diameters may occur under conditions of high shear rates. However, it exhibits non-Newtonian behaviour when it traverses narrow arteries and encounters moderate shear rates, as shown by Rathod and Tanveer [1]. The phenomenon of red blood cells aggregating into the Rouleaux form in response to low shear rates has been shown to lead to an increase in blood viscosity. The blood flow in question has a flattened parabolic velocity profile, deviating from the anticipated parabolic velocity profile seen by Newtonian fluids. The non-Newtonian behaviour seen may be attributed to the existence of a yield stress. The yield stress levels of normal human blood vary between 0.01 and 0.06 dyn/cm<sup>2</sup>, with variations seen according to the blood type studied by Chandran *et al.*, [2]. The phenomenon of blood flow in narrow arteries at low shear rates may be well described by the Casson fluid characteristics, as suggested by Blair [3].

Furthermore, in his study on blood flow, Casson [4] examined the reliability of the Casson fluid model and determined that the yield stress for blood remains non-zero even at low shear rates. The statement mentioned above was derived from an observation made by the researcher throughout the course of their investigation. The experiment conducted by Merrill *et al.*, [5] supports the validity of the Casson fluid model in describing blood flow in tubes with diameters ranging from 130 to 1000  $\mu$ m. The study done by Charm and Kurland [6] provides robust evidence in favour of the Casson fluid model, which offers predictions about the flow of blood in narrow arteries under external pressure. The analysis of the pulsatile flow of Casson fluid via stenosed arteries using the perturbation technique was conducted by Chaturani and Samy [7]. The phenomenon of water flow across a wedge has been investigated by Madhu and Kishan [8]. The MHD flow of Casson nanofluid, driven by aligned magnetic fields, has been investigated by Kalaivanan *et al.*, [9]. In their study, Jain and Parmar [10], as well as Ganga *et al.*, [11], conducted investigations on the slip flow behaviour of a Casson fluid across a stretched sheet. Kodi and Obulesu [12] studied the unsteady magnetohydrodynamic (MHD) oscillatory flow of Casson fluid across an inclined vertical porous plate, considering the influence of chemical reaction, heat absorption, and Soret effects. The study conducted by Kodi *et al.*, [13] examined the characteristics of magnetohydrodynamic (MHD) Casson fluid flow across a vertical porous plate, taking into account the influence of heat transport and chemical reaction. The quantitative investigation of the flow of Casson nanofluid across a stretched sheet has been recently conducted by Senapati *et al.*, [14]. The user's text does not contain any information to be rewritten.

The Hall Effect is primarily seen in the absolute amplitude and direction of the current density, affecting the magnetic force term. The convective flow problem associated with the magnetic field has significance in the presence of Hall currents due to its relevance in many technical applications such as MHD accelerators, nanotechnological processing, liquid metal-based nuclear energy systems, control of blood flow, and heating components. The investigation of magnetohydrodynamic (MHD) flows, including Hall current, is particularly valuable in the examination of Hall accelerators and flight magnetohydrodynamics, especially under conditions when the magnetic field strength is high and the gas density is comparatively low. The use of a magnetic field may induce various applications of peristaltic flows. Several uses may be seen concerning the magnetohydrodynamic properties of blood, the dialysis process, oxygenation, and hypothermia. In recent years, the study of flows involving non-Newtonian fluids has garnered significant interest from specialists due to its wide-ranging potential applications in several industrial and technical domains. Critical applications may be found in several domains, such as food engineering, petroleum production, power engineering, and plastic processing industries involving polymer solutions and melt. The Hall Effect has a notable influence when the Hall parameter assumes a high value. The parameter that characterises the ratio between the electron cyclotron frequency and the atom-electron collision frequency is often referred to as the Hall parameter. The study conducted by Alam *et al.*, [15] examined the characteristics of a steady magnetohydrodynamic (MHD) boundary layer flow with free convection across a porous

inclined plate. The investigation considered the influence of changing suction, the Soret effect, and the existence of the Hall current. In a study conducted by Abo-Eldahab [16], an investigation was carried out on the free convective magnetohydrodynamic (MHD) flow, considering the influence of Hall effects. The study focused on a stretched sheet as the basis for analysis. Thamizsudar's *et al.*, [17] research work focused on examining the impact of Hall current and rotation on the rate of heat and mass transfer in a magnetohydrodynamic (MHD) fluid as it traverses a vertically oriented plate with exponential acceleration. Gopalam and Annareddy [18] used the spectrum relaxation method to investigate the mixed convection flow of nanofluid, considering the influences of Hall and ion-slip phenomena. The impact of a Hall current on a one-dimensional unsteady magnetohydrodynamic (MHD) micropolar fluid flow was explored by Islam *et al.*, [19].

In their study, Kodi *et al.*, [20] investigated the chemically reactive second grade attained inside the porous saturated zone by using a perturbation technique. Raghunath *et al.*, [21] have examined the effects of Soret, Rotation, Hall, and Ion Slip on the unsteady flow of a Jeffrey fluid through a porous medium. The results of their research may be seen in the next section. The study conducted by Raghunath and Mohanaramana [22] investigated the impact of Hall, Soret, and rotational effects on the unsteady magnetohydrodynamic (MHD) rotating flow of a second-grade fluid through a porous media in the presence of a chemical reaction and an aligned magnetic field. In their research, Bafakeeh *et al.*, [23] investigated the impact of Hall current and Soret effects on the unsteady magnetohydrodynamic (MHD) rotating flow of a second-grade fluid through porous media. The study also included the influences of thermal radiation and chemical reactions. The study conducted by Deepthi *et al.*, [24] examined the recent advancements in heat and mass transport in the presence of Hall Effect, ion slip, and thermo diffusion in radiative second-grade materials. The research focused on the use of micromachines in this context. In their study, Ganjikunta *et al.*, [25] investigated the characteristics of an unsteady magnetohydrodynamic (MHD) flow of a second-grade fluid as it traverses a porous media. The analysis also included the influence of radiation absorption, as well as the existence of Hall and ion slip effects.

Thermal radiation has a substantial role in heat dissipation from the surface. Examples of industrial sectors that might potentially profit from the deployment of this technology include helicopters, space vehicles, equipment design with high reliability, satellites, atomic furnaces, missiles, space technologies, and procedures involving high temperatures. The study conducted by Reddy *et al.*, [26] examined the impact of thermal radiation and suction effects on the boundary layer flow of MHD Nanofluid over a nonlinearly stretched sheet. The phenomenon of peristaltic transport inside a tapered asymmetric channel of a Williamson Nanofluid was documented by Kothandapani and Prakash [27], taking into consideration the influence of heat radiation. The effects of Soret and suction/blowing on the magnetohydrodynamic (MHD) stagnation point flow of a radiative Carreau nanofluid over a stretched surface were analysed by Sulochana *et al.*, [28] in their paper. In their study, Kho *et al.*, [29] investigated the impact of radiation on the magnetohydrodynamic (MHD) heat and mass transfer in the context of Casson Nanofluid flow across a porous stretched sheet. In a study conducted by Raza [30], thermal radiation and slip effects on magnetohydrodynamic (MHD) stagnation point flow of Casson fluid over a convective stretching sheet.

Examining the generation and assimilation of thermal energy as a fundamental attribute of fluid flow is imperative because of diverse physical phenomena. The presence of inconsistent heat output has a substantial role in the challenges associated with heat dissipation. Due to the fast progression of electronic technology, there has been an emergence of more efficient cooling techniques for electronic equipment. These technologies have shown efficacy in cooling diverse electronic equipment and are implemented via distinct transistors for mainframes and power supplies for telephone switches. The impact of heat generation and absorption is of utmost significance in

determining the thermal efficiency of base fluids. The versatility of this phenomenon may be seen across a range of situations, including the dissipation of heat from residual nuclear fuel, food preservation, the production of plastic and rubber sheets, the movement of fluids in fixed bed reactors, and several other scenarios. In a recent study conducted by Raghunath *et al.*, [31], the researchers investigated the impact of heat absorption on flow geometries that exhibit variations. In their study, Kumar and Singh [32] investigated the impact of a heat source/sink on the characteristics of magnetohydrodynamic (MHD) stable laminar boundary layer natural convection flow over a vertically oriented circular annulus region. In a study conducted by Bataller [33], an analysis was performed to investigate the impact of heat transport, radiation, heat sources, and heat sinks on a viscoelastic fluid situated on a stretched surface.

The current study builds upon the previous research conducted by Gopalam and Annareddy [18]. This study investigates the influence of Hall current, diffusion thermo, and activation energy on the flow of an electrically conducting Jeffrey nanofluid past a vertical surface, considering the effects of chemical reaction and thermal radiation. Using similarity transformation, the governing partial nonlinear differential equations about flow, heat transport, and mass transfer are transformed into ordinary differential equations. Subsequently, the issues are resolved by numerical methods. This study examines the effects of several non-dimensional regulating parameters on the profiles of velocity, temperature, and concentration. These effects are analysed and graphically shown. The results of the present study demonstrate a high degree of agreement with findings from previous research under certain conditions.

## 2. Formulation of the Problem

In this study, it was assumed that the flow of an immiscible hydromagnetic Jeffrey nanofluid along a longitudinal stretching sheet in the plane  $y = 0$  was steady in heat and mass transfer. At the same time, Hall current consequences were also considered. When the origin is held constant, it is assumed that two forces along the  $x$ -axis will act in opposition to one another and equal measure. As a result, the sheet will stretch linearly in both the positive and negative directions (see Figure 1). A strong magnetic field has been imposed in an order that is normal to the flow direction on the presumption that the Newtonian nanofluid is electrically conductive and capable of producing or absorbing heat. Also, it was thought that there was no electric field and that the frequency of atom-electron collisions had to be pretty high for the Hall current effect to happen [34]. Because of the high magnetic flux density  $B_0$ , the Hall present effect is considered. But the relatively low magnetic Reynolds number is used, and the magnetic field caused by the magnet is not considered. The solid magnetic flux density,  $B_0$ , brings both of these factors.

The Hall current consequence is powerful enough to cause a force to be exerted in the  $z$ -direction. Simultaneously, a cross-flow is induced in the same direction, resulting in a three-dimensional flow. Also, it is assumed that the flow, heat transfer, and mass transfer in the  $z$ -direction are all the same. Considering the sheet that has an infinite width is one way to accomplish this assumption. When a plate that doesn't conduct electricity is considered, the generalized version of Ohm's law shows  $y = 0$  in the flow field [35]. The Brownian motion and thermophoresis effects are considered in the Buongiorno model, which is used to model the nanofluid. In addition, we do not consider the effects of viscous dissipation or Joule heating [36]. The equations that govern the system and the constraints that correspond to them were given by Gopalam and Annareddy [18].

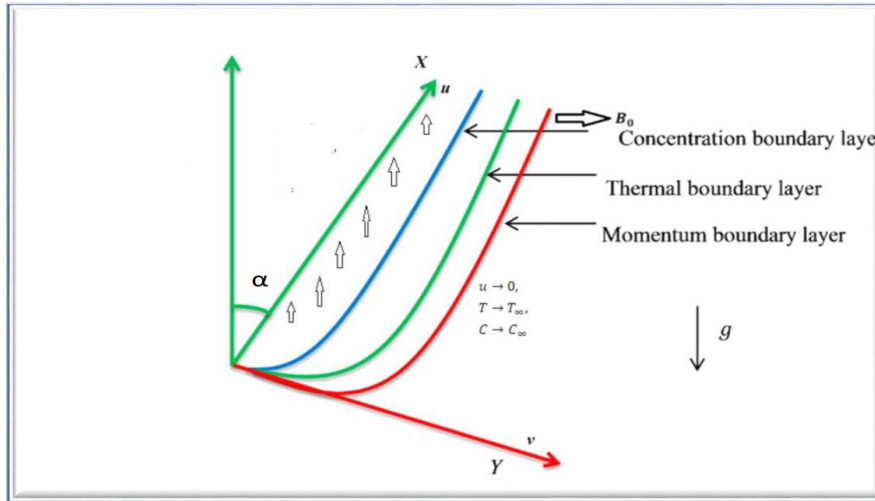


Fig. 1. Configuration of the issue from a physical standpoint

In light of the premises discussed earlier and the Boussinesq approach, the following is the arithmetical representation of the problem.

$$\frac{\partial u}{\partial x} + \frac{\partial u}{\partial y} = 0 \quad (1)$$

$$u \frac{\partial u}{\partial x} + v \frac{\partial u}{\partial y} = \nu \left( \frac{1}{1+\beta} \right) \frac{\partial^2 u}{\partial y^2} - \frac{\sigma B_0^2}{\rho(1+m^2)} (mw + u) + g_c [\beta_T (T - T_\infty) + \beta_C (C - C_\infty)] \cos \alpha \quad (2)$$

$$u \frac{\partial w}{\partial x} + v \frac{\partial w}{\partial y} = \nu \left( \frac{1}{1+\beta} \right) \frac{\partial^2 w}{\partial y^2} + \frac{\sigma B_0^2}{\rho(1+m^2)} (mu - w) \quad (3)$$

$$u \frac{\partial T}{\partial x} + v \frac{\partial T}{\partial y} = \frac{k}{\rho C_p} \frac{\partial^2 T}{\partial y^2} + \frac{Q_0}{\rho C_p} (T - T_\infty) + \tau \left( D_B \frac{\partial C}{\partial y} \frac{\partial T}{\partial y} + \frac{D_T}{T_\infty} \left( \frac{\partial T}{\partial y} \right)^2 \right) - \frac{1}{\rho C_p} \frac{\partial q_r}{\partial y} + \frac{D_m k_T}{c_s c_p} \frac{\partial^2 C}{\partial y^2} \quad (4)$$

$$u \frac{\partial C}{\partial x} + v \frac{\partial C}{\partial y} = D_B \frac{\partial^2 C}{\partial y^2} + \frac{D_T}{T_\infty} \frac{\partial^2 T}{\partial y^2} - k_r^2 (C - C_\infty) \left( \frac{T}{T_\infty} \right)^m \exp \left( \frac{-E_a}{K^* T} \right) \quad (5)$$

The associated boundary conditions for the PDEs that are in charge are as follows:

$$\begin{aligned} u = ax, \quad v = 0, \quad w = 0, \quad T = T_w, \quad C = C_w & \quad \text{at } y = 0 \\ u \rightarrow 0, \quad v \rightarrow 0, \quad w \rightarrow 0, \quad T \rightarrow T_\infty, \quad C \rightarrow C_\infty & \quad \text{as } y \rightarrow \infty \end{aligned} \quad (6)$$

The similarity conversion that was used so that the PDEs may be translated into dimensionless ODEs

$$\eta = \sqrt{\frac{a}{\nu}} y, \quad \psi(x, y) = \sqrt{a\nu} x f(\eta), \quad w = ax g(\eta) \quad \phi(\eta) = \frac{C - C_\infty}{C_w - C_\infty}, \quad \theta(\eta) = \frac{T - T_\infty}{T_w - T_\infty} \quad (7)$$

Because an optically thick fluid also engages in self-absorption in contrast to emission, the Rosseland approximation may be used for the radiative heat flux vector  $q_r$ . We can use the Rosseland approximation because the absorption coefficient is often dependent on the wavelength and is substantial. As a result, the value serves as the description of  $q_r$  [37].

$$q_r = \frac{-4\sigma^*}{3k^*} \frac{\partial^2 T^4}{\partial y^2} \quad (8)$$

The Rosseland mean absorption coefficient is expressed by the symbol  $k^*$  in this expression, while the Stefan–Boltzmann characteristic is represented by the symbol  $\sigma_1$ .

Because we are functioning under the premise that the temperature fluctuations within the flow are not particularly important, we can define  $T^4$  as a linear function. This gives us the ability to predict  $T^4$  with high accuracy. We ignore higher-order variables as we proceed with the process of extending  $T^4$  about the temperature of the free stream  $T$  using Taylor's series. A rough estimate may be found in the preceding, which can be obtained from this: The Rosseland mean absorption coefficient is expressed by the symbol  $k^*$  in this expression.

$$T^4 \approx 4T_\infty^3 - 3T_\infty^4 \quad (9)$$

Combining Eq. (8) and Eq. (9), one may arrive at an equation for energy, as shown in the succeeding.

$$u \frac{\partial T}{\partial x} + v \frac{\partial T}{\partial y} = \frac{k}{\rho C_p} \frac{\partial^2 T}{\partial y^2} + \frac{Q_0}{\rho C_p} (T - T_\infty) + \tau \left( D_B \frac{\partial C}{\partial y} \frac{\partial T}{\partial y} + \frac{D_T}{T_\infty} \left( \frac{\partial T}{\partial y} \right)^2 \right) + \frac{16\sigma^* T_\infty^3}{3\rho C_p k^*} \frac{\partial^2 T}{\partial y^2} + \frac{D_m k_T}{c_s c_p} \frac{\partial^2 C}{\partial y^2} \quad (10)$$

Substitute Eq. (7) into Eq. (2), Eq. (3), Eq. (5) and Eq. (10) generate to acquire the succeeding non-dimensional equations.

$$\left( \frac{1}{1 + \beta} \right) f''' + ff'' - f'^2 + [Gr\theta + Gm\phi] \cos\alpha - \frac{M}{1 + m^2} (f' + mg) = 0 \quad (11)$$

$$\left( \frac{1}{1 + \beta} \right) g'' + fg' - f'g + \frac{M}{1 + m^2} (mf' - g) = 0 \quad (12)$$

$$\theta''(1 + RPr) + Pr f\theta' + Pr N_b \left( \theta' \phi' + \frac{N_T}{N_b} \theta'^2 \right) + Pr Q\theta + Pr D_u \phi' = 0 \quad (13)$$

$$\phi'' + \text{Pr} L_e f \phi' + \frac{N_t}{N_b} \theta'' - K_E (1 + \theta)^m \phi \exp\left(\frac{-E}{1 + \theta}\right) = 0 \quad (14)$$

The dimensionless correlated boundary conditions (BCs) are as shadows

$$\begin{aligned} f(0) = 0, \quad f'(0) = 1, \quad g(0) = 0, \quad \theta(0) = 0, \quad \phi(0) = 1 \quad \text{at} \quad \eta = 0 \\ f'(\eta) \rightarrow 0, \quad g(\eta) \rightarrow 0, \quad \theta(\eta) \rightarrow 0, \quad \phi(\eta) \rightarrow 0 \quad \text{as} \quad \eta \rightarrow \infty \end{aligned} \quad (15)$$

The significant parameters are specified in the equations that do not include proportions.

$$\begin{aligned} M = \frac{\sigma B_0^2}{\rho \alpha}, \quad \text{Pr} = \frac{\nu}{\alpha} = \frac{\nu \rho C_p}{k}, \quad L_e = \frac{\alpha}{D_B}, \quad Q = \frac{Q_0}{a \rho C_p}, \quad Gr = \frac{g_c \beta_T (T_w - T_\infty)}{a^2 x}, \\ N_b = \frac{\tau D_B (C_w - C_\infty)}{\nu}, \quad N_t = \frac{\tau D_T (T_w - T_\infty)}{\nu}, \quad Gm = \frac{g_c \beta_C (C_w - C_\infty)}{a^2 x}, \\ R = \frac{16 \sigma^* T_\infty^3}{3 \rho C_p k^*}, \quad K_E = \frac{k_r^2}{c}, \quad E = \frac{E_a}{K^* T_\infty}, \quad Du = \frac{D_M k_T (C_w - C_\infty)}{C_S C_p \nu a^2 (T_w - T_\infty)}, \end{aligned} \quad (16)$$

### 3. Physical Quantities of Interests

The relevant physical parameters that have an impact on the flow are the local skin friction coefficient in the direction of  $x$   $Cf_x$  and the direction of  $z$   $Cf_z$ , the local Nusselt number  $Nu_x$ , and the local Sherwood number  $Sh_x$ . The following explanations apply to these numerical values:

$$Cf_x = \frac{2\tau_{wx}}{\rho(ax)^2}, \quad Cf_z = \frac{2\tau_{wz}}{\rho(ax)^2}, \quad Nu_x = \frac{xq_w}{k(T_w - T_\infty)}, \quad Sh_x = \frac{xj_w}{D_B(C_w - C_\infty)} \quad (17)$$

where  $\tau_{wx}$ ,  $\tau_{wy}$ ,  $q_w$  and  $j_w$  are the wall skin friction, wall heat flux and wall mass flux respectively given by

$$\tau_{wx} = \mu \left[ \frac{\partial u}{\partial y} \right]_{y=0}, \quad \tau_{wz} = \mu \left[ \frac{\partial w}{\partial y} \right]_{y=0}, \quad q_w = -k \left[ \frac{\partial T}{\partial y} \right]_{y=0}, \quad j_w = -D_B \left[ \frac{\partial C}{\partial y} \right]_{y=0} \quad (18)$$

The following is an expression of the factor of skin friction, the Nusselt number, and the Sherwood number in their non-dimensional forms concerning the similarity component:

$$\text{Re}_x^{1/2} Cf_x = 2f''(0), \quad \text{Re}_x^{1/2} Cf_z = 2g'(0), \quad \text{Re}_x^{1/2} Nu_x = -\theta'(0), \quad \text{Re}_x^{1/2} Sh_x = -\phi'(0) \quad (19)$$

### 4. Solution Methodology

The non-linear ODE system (11–14), susceptible to constraints 15, was solved using the shooting technique for various values of the related parameters. We were able to figure out from the graphs that the behavior of the solutions does not change much when the value is greater than 8. Because of this, and based on the results of the computational experiments described above, we are

considering using the range [0,8] as the domain of the issue rather than the range [0,∞ ].We denote f by  $y_1$ , g by  $y_4$ ,  $\theta$  by  $y_6$  and  $\phi$  by  $y_8$  for converting the boundary value problem (11-15) to the following initial value problem consisting of 9 first order differential equations.

$$y_1' = y_2,$$

$$y_2' = y_3,$$

$$y_3' = \frac{1}{\left(\frac{1}{1+\beta}\right)} \left( -y_1 y_3 + y_2^2 - [Gr_x y_6 + Gr_c y_8] \cos \alpha + \frac{M}{1+m^2} (y_2 + m y_4), \right)$$

$$y_4' = y_5,$$

$$y_5' = \frac{1}{\left(1 + \frac{1}{\beta}\right)} \left( y_2 y_4 - y_1 y_5 - \frac{M}{1+m^2} (-y_4 + m y_2) \right),$$

$$y_6' = y_7,$$

$$y_7' = \frac{1}{(1+RPr)} \left( -Pr y_1 y_7 - Pr N_b \left( y_9 y_7 + \frac{N_T}{N_b} y_7^2 \right) - Pr Q y_6 - Pr D_u y_9 \right),$$

$$y_8' = y_9,$$

$$y_{10}' = -Pr L_e y_1 y_9 - \frac{N_t}{N_b} y_7' + y_8 K_E (1+y_6)^m \exp\left(\frac{-E}{1+y_6}\right)$$

## 5. Results and Discussion

Plotting Figure 2 to Figure 27 allows one to see the influence that several different physical factors have on the tangential velocity  $f'(\eta)$ , the transverse velocity  $g(\eta)$ , the nanoparticle concentration  $\phi(\eta)$ , and the temperature  $\theta(\eta)$  profiles. In each and every one of these calculations, unless it was specifically stated differently, we assumed that  $Nb = 0.3$ ,  $Nt = 0.7$ ,  $Pr = 0.71$ ,  $Le = 0.6$ ,  $\beta = 0.5$ ,  $M = 0.5$ ,  $m = 0.2$ ,  $Gr = 0.5$ ,  $Gm = 0.5$ ,  $Q_0 = 0.5$ ,  $R = 1$ ,  $E = 0.5$ ,  $Du = 0.5$ ,  $\alpha = \pi/3$ .

The influence of the magnetic parameter  $M$  on the tangential velocity  $f'(\eta)$ , longitudinal velocity  $g(\eta)$ , temperature  $\theta(\eta)$ , and concentration  $\phi(\eta)$  profiles, respectively, is shown in Figure 2 through Figure 5. The velocity profile  $f'(\eta)$  drops as the values of  $M$  rise, and a similar trend has been seen with the transverse velocity profile  $g(\eta)$ . On the other hand, the temperature profile  $\theta(\eta)$  and the concentration profile  $\phi(\eta)$  increase as  $M$  grows. When  $M$  is increased, a force of drag known as the Lorentz force also rises. As a result of the fact that this force works against the flow of nanofluid, the velocity in the direction of the flow slows down. In addition, since an electrically conducting nanofluid

and a strong magnetic field in an order that is orthogonal to the flow are being examined, an increase in  $M$  will result in an increase in the force in the  $z$ -direction, which will lead to a decrease in the longitudinal velocity profile  $g(\eta)$ .

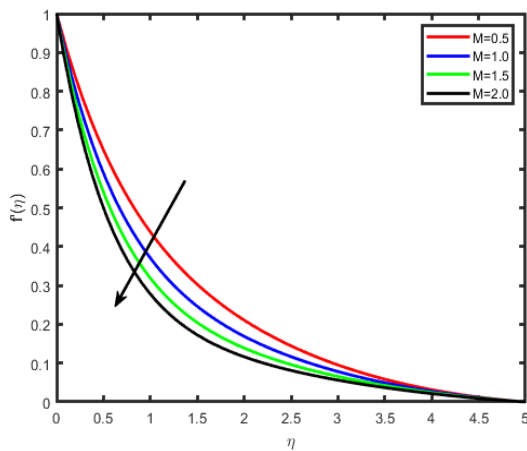


**Fig. 2.** Influence of  $M$  on  $f'(\eta)$

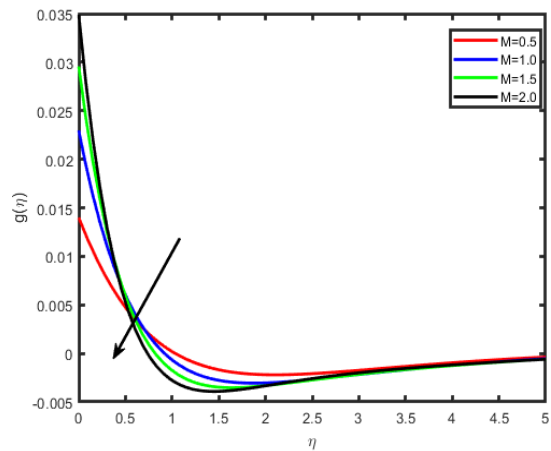


**Fig. 3.** Contribution of  $M$  on  $g(\eta)$

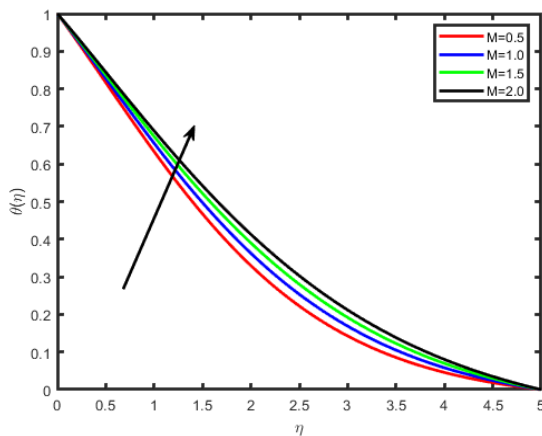


**Fig. 4.** Effect of  $M$  on  $\theta(\eta)$

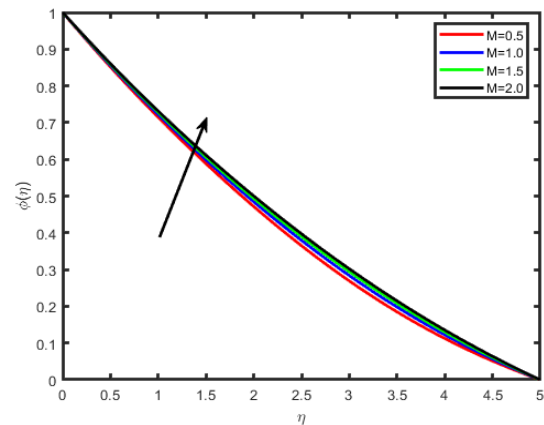


**Fig. 5.** Effect of  $M$  on  $\phi(\eta)$

The effects of the Hall component  $m$  on the tangential velocity  $f^i(\eta)$ , transverse velocity  $g(\eta)$ , nanoparticle concentration  $\phi(\eta)$ , and temperature  $\theta(\eta)$  patterns are depicted in Figure 6 to Figure 9 accordingly. As  $m$  becomes higher, it can be seen in Figure 6 and Figure 7 that the velocity  $f^i(\eta)$  and  $g(\eta)$  profiles go higher as well. On the other hand, Figure 8 and Figure 9 show that both the temperature and concentration curves drop as the distance  $m$  increases. This is because the enclosure of the Hall parameter has the effect of decreasing the effective conductivity, resulting in a diminishing of the resistive force induced by the magnetic field. Therefore, an increase in the Hall factor increases the velocity component.

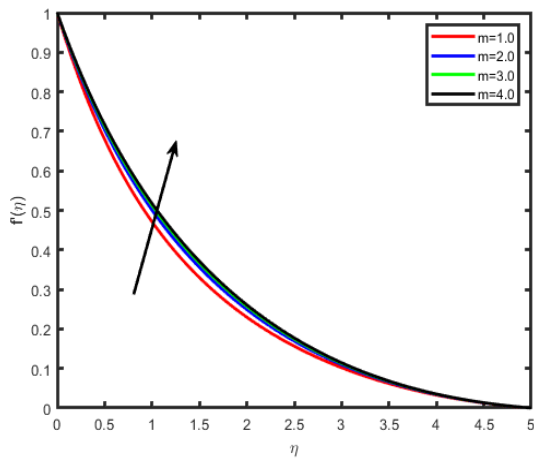


Fig. 6. Influence of  $m$  on  $f'(\eta)$

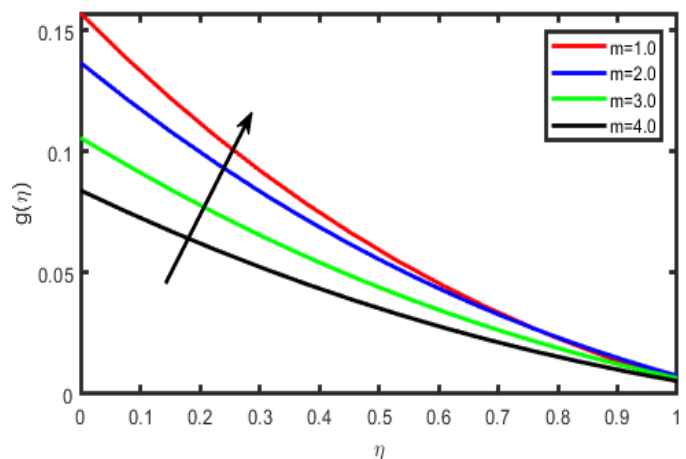


Fig. 7. Contribution of  $m$  on  $g(\eta)$

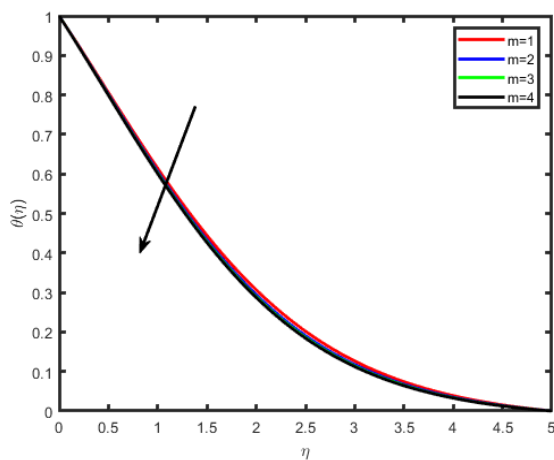


Fig. 8. Effect of  $m$  on  $\theta(\eta)$

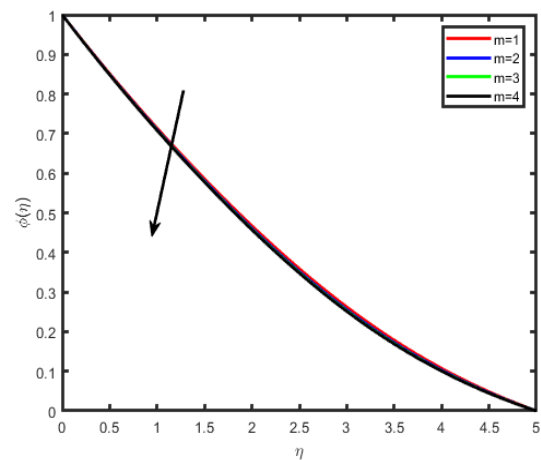
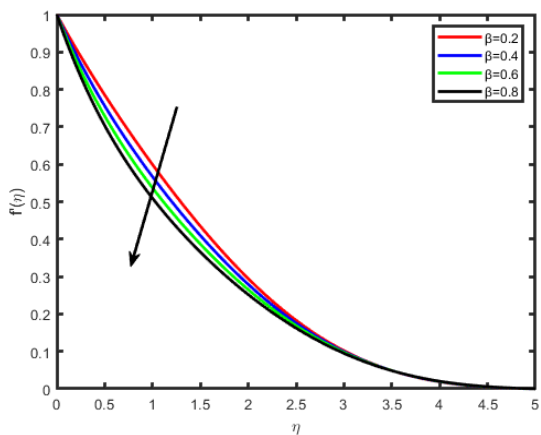
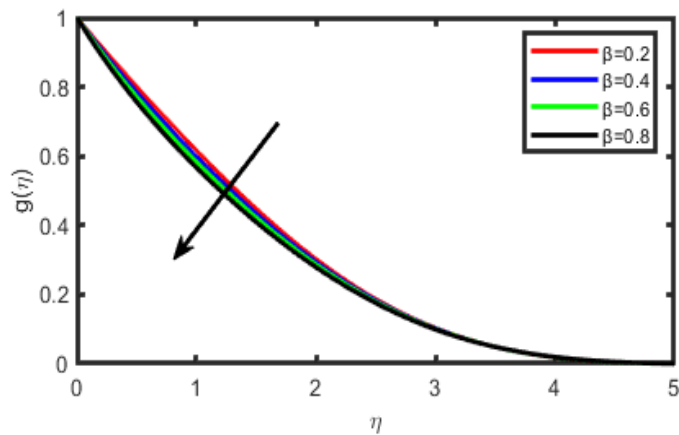


Fig. 9. Influence of  $m$  on  $\phi(\eta)$

The influence that the Jeffrey component ( $\beta$ ) has on the velocity outline is seen in Figure 10 and Figure 11. It has come to our attention that as it grows, the velocity and the thickness of the boundary layer decrease. Therefore, the magnitude of the velocity is more significant in Jeffrey fluid as contrasted to viscous fluids since the Jeffrey fluid is less dense. The consequences of the thermal Grashof  $Gr$  numeral and the mass Grashof  $G_m$  numeral on the tangential velocity  $f''(\eta)$  and the transverse velocity  $g(\eta)$  are correspondingly portrayed in Figure 12 to Figure 15. The Grashof numeral is a ratio of the buoyant force to the viscous force. Because it is assembled as a result of the natural convection flow, it indicates an increase in both the tangential and transverse velocities of the liquid. This occurs because a more significant Grashof number advances a more vital buoyancy force, which in turn means a higher flow movement.



**Fig. 10.** Influence of  $\beta$  on  $f'(\eta)$



**Fig. 11.** Contribution of  $m$  on  $g(\eta)$

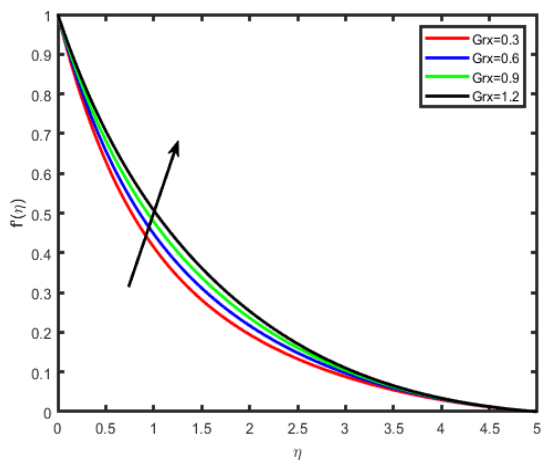


**Fig. 12.** Influence of  $Gr$  on  $f'(\eta)$

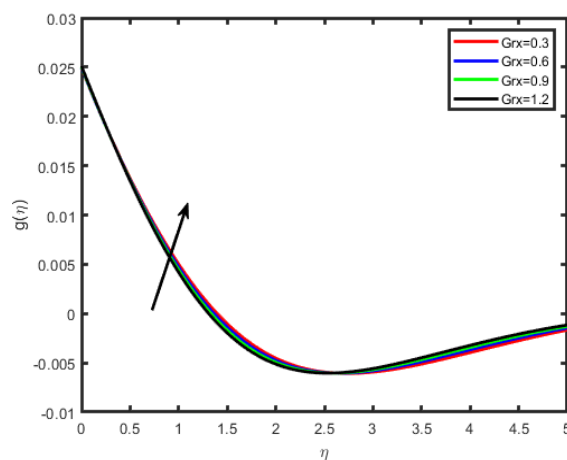


**Fig. 13.** Contribution of  $Gr$  on  $g(\eta)$

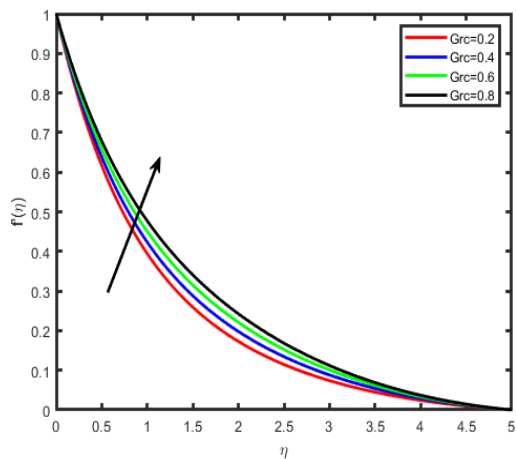


**Fig. 14.** Influence of  $Gm$  on  $f'(\eta)$

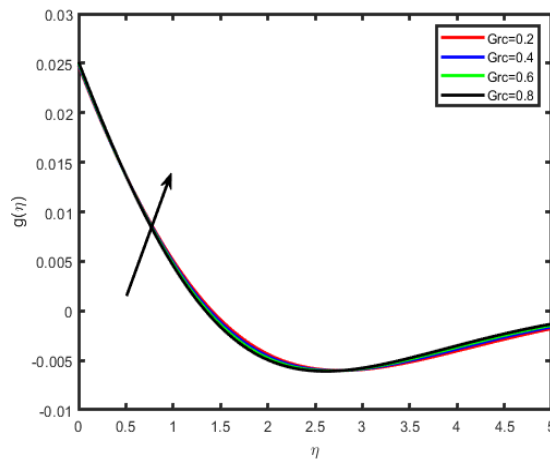


**Fig. 15.** Contribution of  $Gm$  on  $g(\eta)$

The distribution of the thermal radiation factor  $R$ , and Diffusion thermo parameter ( $Du$ ) on temperature sector as seen in Figure 16 and Figure 17. It is interesting to note that a higher value of  $R$  strengthens the temperature. This is because the radiation criterion generates thermal energy in the flow region; as a result, enhancements have been seen in the temperature field. As the Dufour parameter increases, the energy or temperature profiles increases. The Dufour number denotes the contribution of the concentration gradients to the thermal energy flux in the flow. It can be seen that an increase in the Dufour number causes a rise in temperature.

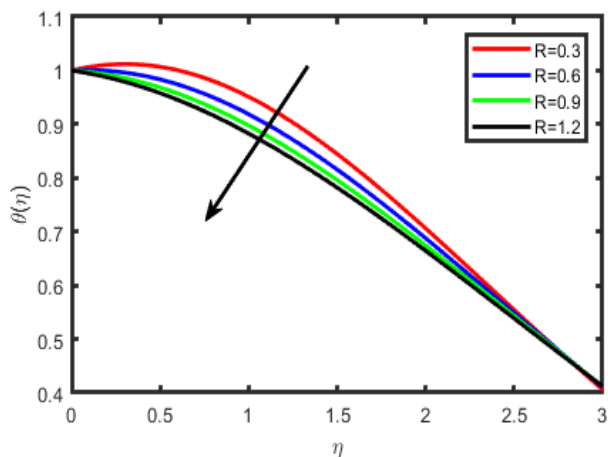


**Fig. 16.** Effect of R on  $\theta(\eta)$

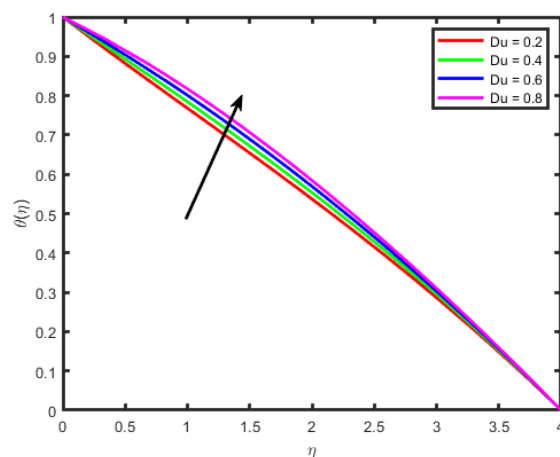


**Fig. 17.** Influence of Du on  $\theta(\eta)$

Figure 18 demonstrates that an elevation in the resistance of the heat source or sink causes an increase in the temperature. This is because an increase in the resistance of heat production causes the temperature to rise. When it comes to focusing, one might expect to see the exact opposite behavior (Figure 19). Figure 20 and Figure 21 provide a study that analyzes the Brownian motion parameter Nb's effect on the temperature and concentration curves. Based on these statistics, we can deduce that an increase in the values of Nb produces a drop in the nanoparticle concentration profile while simultaneously increasing temperature. The Brownian motion refers to the random movement of nanoparticles immersed in a fluid. This motion is induced by the collision of nanoparticles with the particles that make up the fluid. An increase in the thermophoretic effect leads to an increase in the Brownian motion effect, which produces a rise in temperature due to increased kinetic energy.

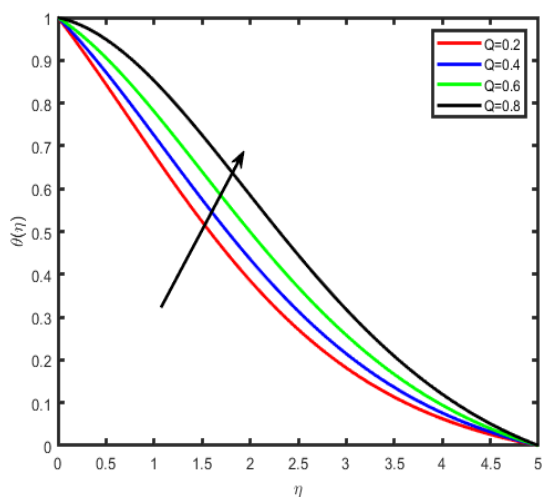


**Fig. 18.** Effect of Q on  $\theta(\eta)$

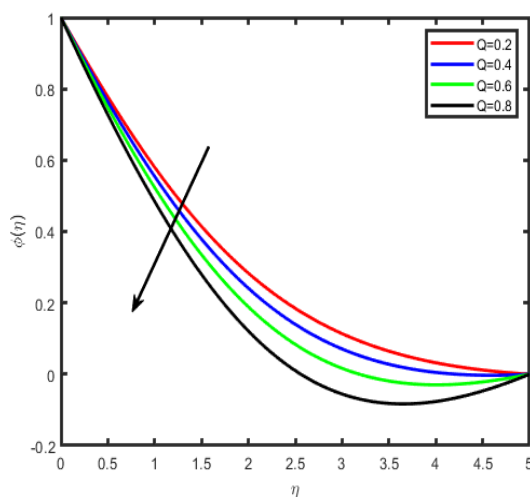


**Fig. 19.** Influence of Q on  $\phi(\eta)$

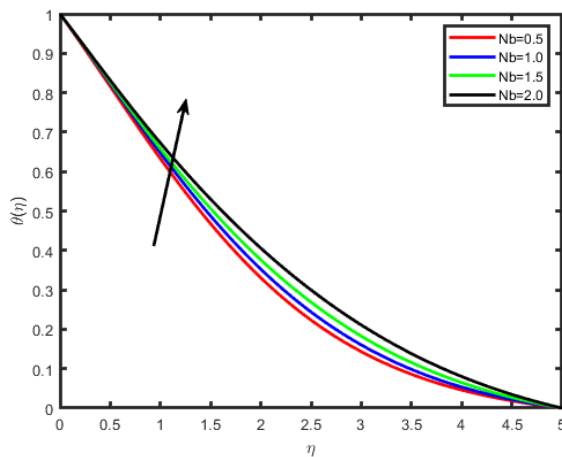


**Fig. 20.** Effect of Nb on  $\theta(n)$

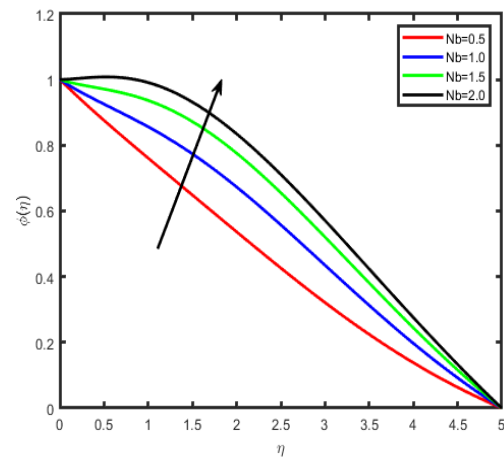


**Fig. 21.** Influence of Nb on  $\phi(n)$

The influence of the thermophoresis parameter  $Nt$  on the temperature and the nanoparticles concentration profile is shown in Figure 22 and Figure 23, respectively. When there is a rise in  $Nt$ , it is possible to notice an increase in the temperature and concentration fields. The thermophoresis parameter is responsible for a substantial part of the flow of heat transfer. When  $Nt$  is raised, the thermophoresis force increases, transporting nanoparticles from the hot zone to the cold region. As a consequence of this movement, the boundary layer's temperature, and thickness rise.

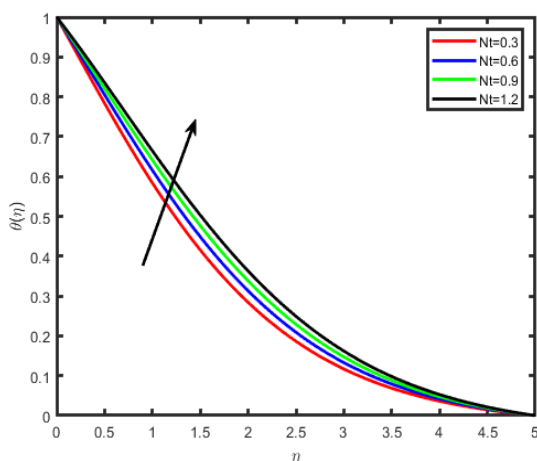


**Fig. 22.** Effect of  $Nt$  on  $\theta(n)$

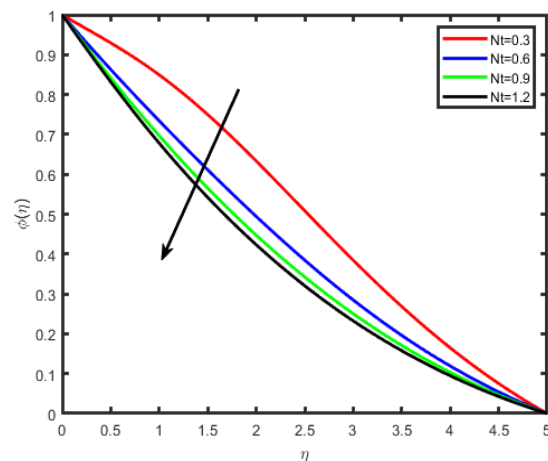


**Fig. 23.** Influence of  $Nt$  on  $\phi(n)$

The Lewis number ( $Le$ ) influence may be seen in Figure 24 and Figure 25, which depict the temperature and nanoparticle concentration trends, respectively. It has been shown that increasing  $Le$  results in a temperature rise while increasing the Lewis number results in a drop in concentration. The influence of the activation energy ( $E$ ) on the concentration field is seen in Figure 26. The graph demonstrates that the concentration profile rises as the value of  $E$  increases. The Arrhenius function degrades due to the activation energy snowballing value, which ultimately leads to the encouragement of the generative chemical reaction, which in turn causes an improvement in the concentration field. When the temperature is low and the activation energy is high, a lower reaction rate constant is produced, which causes the chemical reaction to proceed more slowly. Increased focus is the direct result of this strategy. Figure 27 demonstrates that an increase in the rate of chemical reaction ( $\sigma$ ) causes a significant decrease in the concentration profile. A high chemical reaction rate causes a fallout solute boundary layer to become denser.

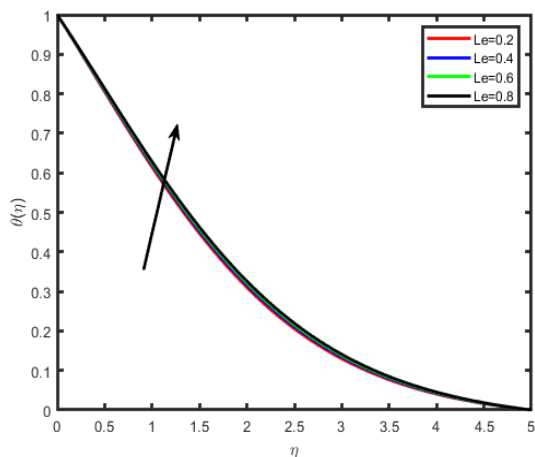


Fig. 24. Effect of Le on  $\theta(n)$

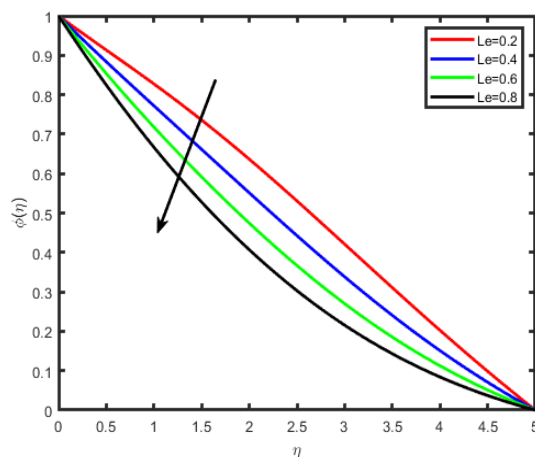


Fig. 25. Influence of Le on  $\phi(n)$

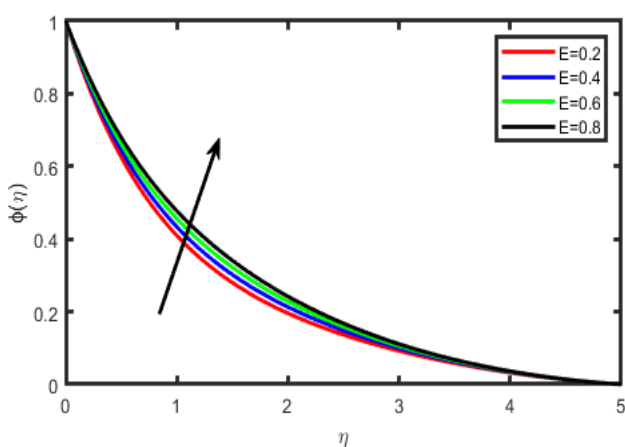


Fig. 26. Influence of E on  $\phi(n)$

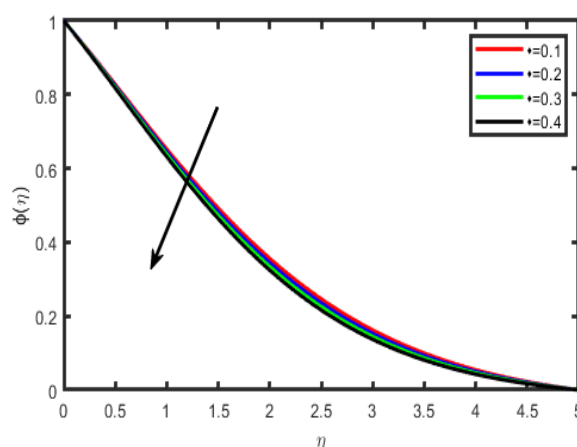


Fig. 27. Influence of  $\sigma$  on  $\phi(n)$

In Table 1, we summarize the effects of various material factors on the local Sherwood numeral, skin friction factor, and local Nusselt numeral. These mathematical results are achieved for the following values of  $Nb = 0.3$ ,  $\beta = 0.5$ ,  $Nt = 0.7$ ,  $Pr = 0.71$ ,  $Le = 0.6$ ,  $M = 0.5$ ,  $m = 0.2$ ,  $Gr = 0.5$ ,  $Gm = 0.5$ ,  $Q = 0.5$ , and  $R = 1$ . It has been seen that the skin-friction coefficient in the x directive decreases with an increase in the thermal Grashof number  $Gr$ , the mass Grashof number  $Gm$ , the Hall current factor  $m$ , and the Brownian motion factor  $Nb$ . On the other hand, it advances with an expansion in the value of the magnetic factor  $M$ , the heat source factor, the radiation, the Prandtl number  $Pr$ , and the thermophoresis parameter  $Nt$ . In the z-direction, the coefficient of the skin's friction behaves differently than in any other direction. When the value of the Hall current parameter  $m$ , the thermal Grashof number, the mass Grashof number, and the Prandtl number all increase, the Nusselt number goes up; regardless, it goes down when the value of the magnetic field parameter  $M$ , the heat source factor, and the radiation factor are all increased. The Sherwood numeral exhibits an increasing behavior for the thermal Grashof numeral  $Gr$ , the magnetic field factor  $M$ , the Brownian motion factor  $Nb$ , the heat source and radiation factor, and the thermophoresis parameter  $Nt$ , whereas the Grashoff numeral  $Gm$  and Prandtl number exhibit a decreasing behavior.

**Table 1**

Numerical values of  $Re_x^{1/2} C_f_x$ ,  $Re_x^{1/2} C_f_z$ ,  $Re_x^{1/2} Nu_x$ ,  $Re_x^{1/2} Sh_x$

Gr	Gm	Q	m	Nb	R	M	Pr	Nt	$-2f''(0)$	$-2g'(0)$	$-\theta'(0)$	$-\phi'(0)$
0.50									1.25430	0.85240	0.52121	0.95140
1.00									0.99720	0.96730	0.53232	0.99127
1.50									0.73550	0.99230	0.54579	1.02456
	0.30								0.98630	0.88330	0.503207	0.12475
	0.60								0.84750	0.98350	0.51246	0.11083
	0.90								0.71210	1.28730	0.57854	0.91784
			1.0						1.52930	0.85830	0.31453	0.88525
			2.0						1.02930	0.99370	0.29782	0.79523
			3.0						0.82720	0.99850	0.23123	0.94522
				0.20					0.90380	0.95210	0.84525	0.58523
				0.40					0.88350	0.96120	0.82156	0.61244
				0.60					0.79830	0.98520	0.80327	0.69785
						0.50			0.96720	1.02540	0.98758	0.78526
						1.00			1.22760	0.98520	0.91259	0.89527
						1.50			1.46240	0.85120	0.89525	0.94525
							0.680		0.99250	1.02140	0.12544	0.98784
							0.710		0.98730	0.98520	0.15783	0.94523
							0.760		0.83860	0.90320	0.19873	0.92312
								0.30	1.59350	0.98520	0.85422	0.51203
								0.60	1.18370	0.91200	0.81254	0.59214
								0.90	0.89370	0.89620	0.75215	0.61205
		0.20							0.78360	0.98750	0.95426	0.98526
		0.40							0.78520	0.94520	0.91254	0.97454
		0.60							0.8930	0.91320	0.86573	0.96453
					0.50				0.87520	1.08750	0.74522	0.91242
					1.00				0.89520	0.94420	0.73651	0.91203
					1.50				0.91250	0.91140	0.71548	0.91024

As part of the process to validate the numerical approach that was used, the results were compared to those that had been achieved in the past by Gopalam and Annareddy [18] for a variety of parameter values, and the result reveals that there is a good concordance, as can be seen in Table 2.

**Table 2**

Comparison of  $-\theta'(0)$  for various values of Pr when Nb= 0.30, Nt= 0.70, Pr= 0.710, Le = 0.60, M= 0.50, Gr = 0.50, Gm= 0.50, m=0.50, Q=1.00, R=0.50  $\beta=Du=0$

Pr	Gopalam and Annareddy [18]	Present values
0.010	0.0198	0.0188
0.720	0.8072	0.8091
1.0	1.0001	1.0000
3.0	1.9243	1.9231
10.0	3.7321	3.7364

## 6. Conclusion

The effects of the Hall current and thermal radiation on nanofluids' heat and mass transfer flow over a linearly stretched sheet in the presence of heat sources and sinks are investigated. In this study, we will be talking about thermophoresis and Brownian motion. The following are the several categories that have been established to describe the most significant achievements.

As the Jeffrey fluid parameter ( $\beta$ ) increases, there is a corresponding decrease in the fluid's resultant velocity. The temperature rises with the values of the heat source/sink parameter (Q), Diffusion thermo Parameter (Du) and the Brownian motion parameter (Nb), yet the concentration profile of nanoparticles falls. On the other hand, the radiation parameter was shown to have the opposite tendency (R). An increase in the thermophoresis parameter results in an intensification of both the temperature and concentration fields (Nt).

Raising the Prandtl number (Pr) tends to bring about a decrease in both the temperature and concentration profiles. A rise in Le causes an increase in temperature, but an increase in Lewis number causes a drop in concentration. When the hall parameter (m) is increased, the velocity increases, but the opposite trend is shown when temperature and concentration are considered.

## References

- [1] Rathod, V. P., and Shaker Tanveer. "Pulsatile flow of couple stress fluid through a porous medium with periodic body acceleration and magnetic field." *Bulletin of the Malaysian Mathematical Sciences Society* 32, no. 2 (2009).
- [2] Chandran, Krishnan B., Stanley E. Rittgers, and Ajit P. Yoganathan. *Biofluid Mechanics: The Human Circulation*. CRC Press, 2012. <https://doi.org/10.1201/b11709>
- [3] Blair, G. W. Scott. "An equation for the flow of blood, plasma and serum through glass capillaries." *Nature* 183, no. 4661 (1959): 613-614. <https://doi.org/10.1038/183613a0>
- [4] Casson, N. "Flow equation for pigment-oil suspensions of the printing ink-type." *Rheology of Disperse Systems* (1959): 84-104.
- [5] Merrill, E. W., A. M. Benis, E. R. Gilliland, T. K. Sherwood, and E. W. Salzman. "Pressure-flow relations of human blood in hollow fibers at low flow rates." *Journal of Applied Physiology* 20, no. 5 (1965): 954-967. <https://doi.org/10.1152/jappl.1965.20.5.954>
- [6] Charm, S., and G. Kurland. "Viscometry of human blood for shear rates of 0-100,000 sec<sup>-1</sup>." *Nature* 206, no. 4984 (1965): 617-618. <https://doi.org/10.1038/206617a0>
- [7] Chaturani, P., and R. Ponnalagar Samy. "Pulsatile flow of Casson's fluid through stenosed arteries with applications to blood flow." *Biorheology* 23, no. 5 (1986): 499-511. <https://doi.org/10.3233/BIR-1986-23506>
- [8] Madhu, Macha, and Naikoti Kishan. "MHD flow and heat transfer of Casson nanofluid over a wedge." *Mechanics & Industry* 18, no. 2 (2017): 210. <https://doi.org/10.1051/meca/2016030>
- [9] Kalaivanan, R., P. Renuka, N. Vishnu Ganesh, AK Abdul Hakeem, B. Ganga, and S. Saranya. "Effects of aligned magnetic field on slip flow of Casson fluid over a stretching sheet." *Procedia Engineering* 127 (2015): 531-538. <https://doi.org/10.1016/j.proeng.2015.11.341>
- [10] Jain, Shalini, and Amit Parmar. "Multiple slip effects on inclined MHD Casson fluid flow over a permeable stretching surface and a melting surface." *International Journal of Heat and Technology* 36, no. 2 (2018): 585-594. <https://doi.org/10.18280/ijht.360222>
- [11] Ganga, B., M. Govindaraju, and A. K. Abdul Hakeem. "Effects of inclined magnetic field on entropy generation in nanofluid over a stretching sheet with partial slip and nonlinear thermal radiation." *Iranian Journal of Science and Technology, Transactions of Mechanical Engineering* 43 (2019): 707-718. <https://doi.org/10.1007/s40997-018-0227-0>
- [12] Kodi, Raghunath, and Obulesu Mopuri. "Unsteady MHD oscillatory Casson fluid flow past an inclined vertical porous plate in the presence of chemical reaction with heat absorption and Soret effects." *Heat Transfer* 51, no. 1 (2022): 733-752. <https://doi.org/10.1002/htj.22327>
- [13] Kodi, Raghunath, Obulesu Mopuri, Sujatha Sree, and Venkateswaraju Konduru. "Investigation of MHD Casson fluid flow past a vertical porous plate under the influence of thermal diffusion and chemical reaction." *Heat Transfer* 51, no. 1 (2022): 377-394. <https://doi.org/10.1002/htj.22311>
- [14] Senapati, Madhusudan, Kharabela Swain, and Sampad Kumar Parida. "Numerical analysis of three-dimensional MHD flow of Casson nanofluid past an exponentially stretching sheet." *Karbala International Journal of Modern Science* 6, no. 1 (2020): 13. <https://doi.org/10.33640/2405-609X.1462>
- [15] Alam, M. S., M. Ali, M. A. Alim, and A. Saha. "Steady MHD boundary free convective heat and mass transfer flow over an inclined porous plate with variable suction and Soret effect in presence of hall current." *Bangladesh Journal of Scientific and Industrial Research* 49, no. 3 (2014): 155-164. <https://doi.org/10.3329/bjsir.v49i3.22129>
- [16] Abo-Eldahab, Emad M. "Hall effects on magnetohydrodynamic free-convection flow at a stretching surface with a uniform free-stream." *Physica Scripta* 63, no. 1 (2001): 29. <https://doi.org/10.1238/Physica.Regular.063a00029>

- [17] Thamizhsudar, M., J. Pandurangan, and R. Mathucumaraswamy. "Hall effects and rotation effects on MHD flow past an exponentially accelerated vertical plate with combined heat and mass transfer effects." *International Journal of Applied Mechanics and Engineering* 20, no. 3 (2015): 605-616. <https://doi.org/10.1515/ijame-2015-0039>
- [18] Gopalam, Neeraja, and Saila Kumari Annareddy. "Hall Current and Thermal Radiation Effects on MHD Nanofluid in the Presence of Heat Source/Sink, Brownian Motion and Thermophoresis with Inclined Plates." *Journal of Advanced Research in Fluid Mechanics and Thermal Sciences* 104, no. 1 (2023): 152-168. <https://doi.org/10.37934/arfmts.104.1.152168>
- [19] Islam, M. R., M. Asaduzzaman, and M. M. Alam. "Hall current effects on one dimensional unsteady MHD micropolar fluid flow past an impulsive started plate." *International Journal of Engineering Technology Science and Research* 2 (2015): 79-88.
- [20] Kodi, Raghunath, Mohanaramana Ravuri, Nagesh Gulle, Charankumar Ganteda, Sami Ullah Khan, and M. Ijaz Khan. "Hall and ion slip radiative flow of chemically reactive second grade through porous saturated space via perturbation approach." *Waves in Random and Complex Media* (2022): 1-17. <https://doi.org/10.1080/17455030.2022.2108555>
- [21] Raghunath, Kodi, Charankumar Ganteda, and Giulio Lorenzini. "Effects of Soret, rotation, Hall, and ion slip on unsteady MHD flow of a Jeffrey fluid through a porous medium in the presence of heat absorption and chemical reaction." *Journal of Mechanical Engineering Research and Developments* 45, no. 3 (2022): 80-97.
- [22] Raghunath, Kodi, and Ravuri Mohanaramana. "Hall, Soret, and rotational effects on unsteady MHD rotating flow of a second-grade fluid through a porous medium in the presence of chemical reaction and aligned magnetic field." *International Communications in Heat and Mass Transfer* 137 (2022): 106287. <https://doi.org/10.1016/j.icheatmasstransfer.2022.106287>
- [23] Bafakeeh, Omar T., Kodi Raghunath, Farhan Ali, Muhammad Khalid, El Sayed Mohamed Tag-ElDin, Mowffaq Oreijah, Kamel Guedri, Nidhal Ben Khedher, and Muhammad Ijaz Khan. "Hall current and Soret effects on unsteady MHD rotating flow of second-grade fluid through porous media under the influences of thermal radiation and chemical reactions." *Catalysts* 12, no. 10 (2022): 1233. <https://doi.org/10.3390/catal12101233>
- [24] Deepthi, V. V. L., Maha MA Lashin, N. Ravi Kumar, Kodi Raghunath, Farhan Ali, Mowffaq Oreijah, Kamel Guedri, El Sayed Mohamed Tag-ElDin, M. Ijaz Khan, and Ahmed M. Galal. "Recent development of heat and mass transport in the presence of Hall, ion slip and thermo diffusion in radiative second grade material: application of micromachines." *Micromachines* 13, no. 10 (2022): 1566. <https://doi.org/10.3390/mi13101566>
- [25] Ganjikutna, Aruna, Hari Babu Kommaddi, Venkateswarlu Bhajanthri, and Raghunath Kodi. "An unsteady MHD flow of a second-grade fluid passing through a porous medium in the presence of radiation absorption exhibits Hall and ion slip effects." *Heat Transfer* 52, no. 1 (2023): 780-806. <https://doi.org/10.1002/htj.22716>
- [26] Reddy, Yanala Dharmendar, Dodda Ramya, and Laxmianarayanagari Anand Babu. "Effect of thermal radiation on MHD boundary layer flow of nanofluid and heat transfer over a non-linearly stretching sheet with transpiration." *Journal of Nanofluids* 5, no. 6 (2016): 889-897. <https://doi.org/10.1166/jon.2016.1284>
- [27] Kothandapani, M., and J. Prakash. "Effects of thermal radiation parameter and magnetic field on the peristaltic motion of Williamson nanofluids in a tapered asymmetric channel." *International Journal of Heat and Mass Transfer* 81 (2015): 234-245. <https://doi.org/10.1016/j.ijheatmasstransfer.2014.09.062>
- [28] Sulochana, C., S. Payad Samrat, and N. Sandeep. "Thermal radiation effect on MHD nanofluid flow over a stretching sheet." *International Journal of Engineering Research in Africa* 23 (2016): 89-102. <https://doi.org/10.4028/www.scientific.net/JERA.23.89>
- [29] Kho, Yap Bing, Abid Hussanan, Norhafizah Mohd Sarif, Zulkhibri Ismail, and Mohd Zuki Salleh. "Thermal radiation effects on MHD with flow heat and mass transfer in Casson nanofluid over a stretching sheet." In *MATEC Web of Conferences*, vol. 150, p. 06036. EDP Sciences, 2018. <https://doi.org/10.1051/mateconf/201815006036>
- [30] Raza, Jawad. "Thermal radiation and slip effects on magnetohydrodynamic (MHD) stagnation point flow of Casson fluid over a convective stretching sheet." *Propulsion and Power Research* 8, no. 2 (2019): 138-146. <https://doi.org/10.1016/j.jprr.2019.01.004>
- [31] Raghunath, Kodi, Nagesh Gulle, Ramachandra Reddy Vaddemani, and Obulesu Mopuri. "Unsteady MHD fluid flow past an inclined vertical porous plate in the presence of chemical reaction with aligned magnetic field, radiation, and Soret effects." *Heat Transfer* 51, no. 3 (2022): 2742-2760. <https://doi.org/10.1002/htj.22423>
- [32] Kumar, Dileep, and A. K. Singh. "Effects of heat source/sink and induced magnetic field on natural convective flow in vertical concentric annuli." *Alexandria Engineering Journal* 55, no. 4 (2016): 3125-3133. <https://doi.org/10.1016/j.aej.2016.08.019>
- [33] Bataller, Rafael Cortell. "Effects of heat source/sink, radiation and work done by deformation on flow and heat transfer of a viscoelastic fluid over a stretching sheet." *Computers & Mathematics with Applications* 53, no. 2 (2007): 305-316. <https://doi.org/10.1016/j.camwa.2006.02.041>
- [34] Sutton, George W., and Arthur Sherman. *Engineering magnetohydrodynamics*. McGraw-Hill, 1965.

- [35] Abo-Eldahab, Emad M., and Mohamed A. El Aziz. "Hall and ion-slip effects on MHD free convective heat generating flow past a semi-infinite vertical flat plate." *Physica Scripta* 61, no. 3 (2000): 344. <https://doi.org/10.1238/Physica.Regular.061a00344>
- [36] Buongiorno, Jacopo. "Convective transport in nanofluids." *ASME Journal of Heat and Mass Transfer* 128, no. 3 (2006): 240-250. <https://doi.org/10.1115/1.2150834>
- [37] Reddy, Nalivela Nagi, Vempati Srinivasa Rao, and B. Ravindra Reddy. "Impact of thermal radiation and chemical reaction on MHD heat and mass transfer Casson nanofluid flow past a stretching sheet in presence of heat source/sink." *ARPJ Journal of Engineering and Applied Sciences* 16 (2006): 1165-1172.